JOURNAL OF MECHANICAL ENGINEERING AND SCIENCES
ISSN: 2289-4659 e-ISSN: 2231-8380
VOLUME 19, ISSUE 2, 2025, 10577 - 10593
DOI: https://doi.org/10.15282/jmes.19.2.2025.1.0829

RESEARCH ARTICLE

Optimized design and performance analysis of a high-pressure radial turbine for energy recovery applications

N. S. Ahmad[1], M. N. Azman[1], A. M. I. Bin Mamat[1,2]*

[1] College of Engineering, Universiti Teknologi MARA, 40450, Shah Alam, Selangor Darul Ehsan, Malaysia
[2] Smart Manufacturing Research Institute (SMRI), Universiti Teknologi MARA, 40450, Shah Alam, Selangor Darul Ehsan, Malaysia
Phone: +6035543 5251; Fax.: +6015543 5052

ABSTRACT - Single-cylinder direct-injection engines suffer significant exhaust energy losses; however, designing efficient radial turbines for such systems requires a physical characterization of pulsating flows and thermal stresses. This paper investigates the design and performance of a 500W high-pressure radial turbine for waste energy recovery for a single-cylinder engine. The main objective of this study is to optimize the turbine's dimensions and efficiency for capturing exhaust energy upstream of catalytic converters in internal combustion engines. Employing a two-stage computational approach, numerical modeling first established key geometric parameters, including a 19.3 mm inlet radius, 5.1 mm leading-edge length, 72° inlet angle, and 0.7 outlet radius ratio, followed by CFD simulations in ANSYS CFX using a 212,212-element single-passage mesh at 50,000, 70,000 rpm and 90,000 rpm, and 800 K inlet temperature. The optimized turbine demonstrated peak efficiency of 67% at a mass flow rate of 0.005 kg/s, revealing that systematic numerical optimization significantly enhances energy conversion efficiency. These results provide critical insights for developing compact, high-efficiency turbines for exhaust energy recovery systems, advancing waste heat utilization technology.

ARTICLE HISTORY

Received	:	11th Sept. 2024
Revised	:	06th May 2025
Accepted	:	10th June 2025
Published	:	30th June 2025

KEYWORDS
Turbomachinery
Radial turbine
Numerical analysis
CFD analysis

1. INTRODUCTION

The internal combustion engine produces greenhouse gases (GHGs) from the combustion process. The application of biofuels can reduce these harmful GHGs [1]. Although biofuels only decrease GHGs, they cannot increase engine performance. Increasing the air intake pressure will increase the engine performance and power output [2]. The supercharging system, which either applies supercharging or turbocharging in the internal combustion engine, increases the intake air pressure. In the turbocharging system, the exhaust energy is expanded in the radial turbine to generate mechanical power, which drives the compressor's impeller. This impeller compresses the air intake, increasing air density [3]. Significant attention to improving the efficiency and power output of internal combustion engine research has led to an investigation of the turbocharging system and radial turbines, due to their potential to enhance the engine's performance [4]. The air density entering the combustion chamber is increased by using the turbocharging system. Therefore, the power of the internal combustion engine is boosted. The major component of the turbocharging system that enhances its effectiveness is the centrifugal compressor, which is powered by the kinetic energy of the exhaust gases that would otherwise be wasted [3]. This energy is utilised to raise more air mass to enter the combustion chamber by increasing the intake air pressure, thus improving the engine's overall fuel efficiency [5].

The radial turbines are another crucial component of the turbocharging system. To comprehend the fundamental correlation of radial turbine design, extensive studies have been conducted to increase energy transfer efficiency for various applications, including turbochargers, small power plants, and aircraft engines. The fundamental design of radial turbines includes the fluid entering radially and then being guided through a set of blades, which leads to the rotation of the rotor and the generation of mechanical energy [6]. The major factor in the current radial turbine design is to obtain suitable design parameters that meet the operating requirements. Commercial design software for turbomachinery often lacks performance analysis to aid designers in making informed decisions. Integrating computational fluid dynamics into the turbomachinery design will assist the design process and reduce the design timeframe. Optimizing these parameters is crucial for enhancing their performance and efficiency, and this process requires careful evaluation of their dimensions, geometry, and other relevant factors during the design phase [7]. The volute of the radial turbine is correlated with the Area Ratio, A/R, of the volute and turbine design [8, 9]. The turbine's geometric configuration can be generated using the Bezier curve method [10].

The turbomachinery design process is inherently complex, often beginning with defining initial design requirements and progressing through phases that involve modifying geometric parameters with parametric variations [11]. The design process is typically followed by simple calculations, assuming steady and one-dimensional flow, which allows for investigating a limited set of design options [12]. However, as highlighted by Noughabi and Sammak [13], a more detailed design and analysis approach is necessary for radial turbines, which generally involves defining the turbine's geometry

***CORRESPONDING AUTHOR | A. M. I. Bin Mamat |** ✉ amanihsan@uitm.edu.my

and making state assumptions on losses to calculate efficiency. This procedure helps estimate key performance parameters, such as expansion ratio, mass flow rate, power output, and efficiency, producing a performance map for the turbomachinery design. The performance map is a characteristic of the designed turbomachinery and can be scaled up or down according to the requirements [14].

Integrating Computational Fluid Dynamics (CFD) in the radial turbine design is critical to improving the design process. The CFD tool has become essential in fluid mechanics for predicting mass and heat transfer, fluid movement, and related phenomena. The software enables the analysis and resolution of fluid flow issues with high accuracy. Therefore, the study's outcome can be used to improve turbomachinery design. However, the effectiveness of CFD models heavily depends on their precision, and there are inherent limitations, such as the simplifications made to reduce computational demands [15]. Despite the advantages of CFD, traditional methods such as Reynolds-Averaged Navier-Stokes (RANS) and Unsteady Reynolds-Averaged Navier-Stokes (URANS) have limitations, particularly in heat transport and turbulence modelling [16]. These limitations often necessitate simplifications of geometric and operating conditions, which can affect the accuracy of the simulations. However, CFD remains a powerful tool for understanding the internal flow behaviour within turbomachines and for designing and producing efficient machines for various industrial applications. A single passage analysis for the radial turbine can minimize computational time and efficiently analyze the internal flow in the radial turbine [17]. Structural strength requirements limit radial turbine aerodynamics by restricting blade speed and pressure ratios. However, mixed-flow designs with non-radial fibre orientation reduce centrifugal stress, enabling higher performance without material advances [17].

Several studies have demonstrated the application of CFD in turbomachinery analysis. For instance, Borovkov et al. [18] employed CFD simulations to predict the aerodynamic performance of a low-speed impeller, while Yu et al. [19] used CFD to investigate the aerothermodynamic performance of the turbomachinery design for a turbocharging system in an internal combustion engine. These studies emphasize the importance of CFD in optimizing turbomachinery components, particularly in scenarios where traditional experimental methods are impractical or too costly. Additionally, in off-design operating conditions, using CFD to analyze the flow phenomena in high-pressure turbines is significant for understanding and identifying possible solutions. Some solutions require a complex blade design, necessitating challenging high-fidelity CFD modeling [20]. The relationship between flow behavior and turbine performance under various off-design operating conditions can be examined using CFD, making it a critical tool for optimizing turbine design [21]. Bin Mamat et al. [12] used CFD to evaluate the correlation between the flow behavior in the passage and turbine performance, and to optimize the Low-Pressure Turbine design point. The study employed a single passage CFD to determine the inlet absolute angle, $\alpha 1$, at the design point.

In summary, the literature highlights the crucial role of turbochargers and radial turbines in improving the performance of internal combustion engines. While traditional design methods and one-dimensional analyses provide a foundational understanding, integrating CFD in the design and analysis process offers a more detailed and accurate approach to optimizing these components. The continued advancement of CFD techniques and their application in turbomachinery design is essential for further improving the efficiency and performance of these systems. The primary objective of this paper is to present a comprehensive method for designing a low-energy radial turbine by integrating one-dimensional turbine modeling with the CFD technique. The first part presents a numerical one-dimensional rotor design that implements theoretical equations from turbomachinery, fluid mechanics, and thermodynamics. Thereafter, the turbine rotor design was constructed in a three-dimensional virtual design. Finally, Ansys CFX was used to evaluate the turbine off-design operating performance.

2. MATERIALS AND METHODS

2.1 Numerical Rotor Design

The radial turbine rotor transfers energy from the hot gas, and the design process typically starts from the Euler turbomachinery equation. This study employed a systematic method to establish the basic design. The approach accelerated progress toward the ultimate objective by implementing a starting point design, streamlining the overall design and optimization process. Figure 1 depicts a typical turbine rotor. The rotor blades are typically radial at the inlet, as this configuration optimises stress conditions. Early design procedures for achieving the best efficiency point assumed that the inlet relative velocity vector aligned with the radial blade, resulting in a right-angled velocity triangle. However, experimental data and incidence loss models have shown that a significant angle of incidence occurs at the point of best efficiency, making the velocity triangle more accurate.

At the inlet, it is assumed that the blades were radial. It was discovered that the best efficiency occurred when the flow at the inlet did not exactly match the blade but at some negative incidence. The mismatch is due to the blade loading creating a huge static pressure gradient across each passage, pushing the flow from the pressure to the suction surface in the opposite direction of rotation. As a result, the incidence angle at which the best efficiency occurred had to be determined. The incidence angle of a rotor with radial blades coincides with the angle of approach of the relative velocity vector, β_1 [11]. At the design stage, the fluid is usually believed to be discharged from the rotor in an axial direction. By integrating this Equation with the velocity triangles at the inlet and outlet, an expression for work transfer per unit mass flow is derived based on fluid and rotor velocities. In such cases, the Euler turbomachinery equation looks like this:

$$\frac{\dot{W}_T}{\dot{m}} = U_1 C_{\theta 1} - U_2 C_{\theta 2} = h_{01} - h_{02} \tag{1}$$

$$\frac{\dot{W}_T}{\dot{m}} = \frac{1}{2}[(U_1^2 - U_2^2) - (W_1^2 - W_2^2) + (C_1^2 - C_2^2)] \tag{2}$$

Subscripts 1 and 2 correspond to the rotor inlet and exit planes.

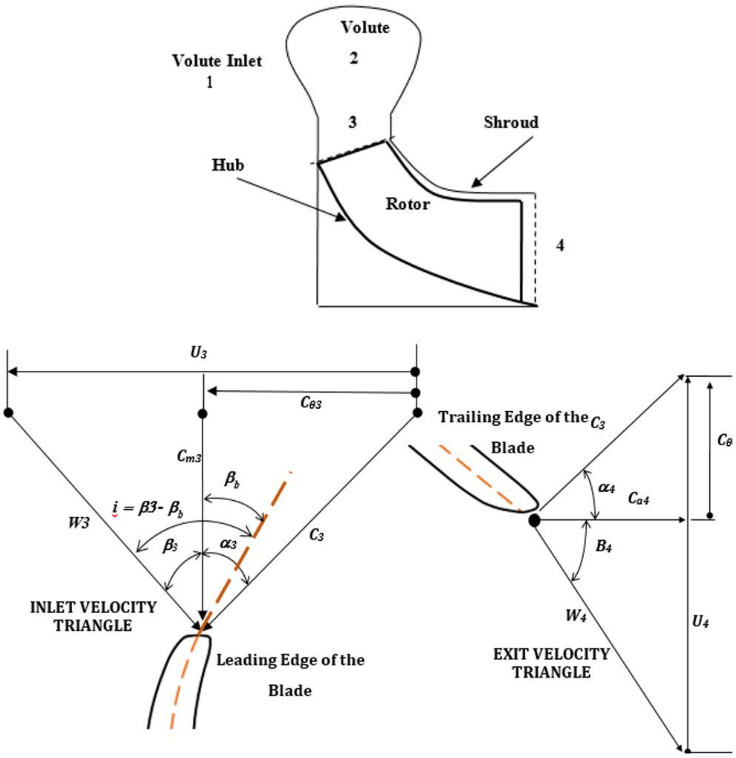

Figure 1. Velocity triangle of a turbine rotor

The objective is to maintain flow velocities as low as possible since various losses, such as friction and exit kinetic energy, increase with the square of velocity. While optimizing for high efficiency focuses primarily on energy utilization, achieving high specific work production is often equally or more important. This scenario necessitates a compromise, as it anticipates higher velocities in particular areas of the machine. The typical configuration of the velocity triangles at the rotor's inlet and outlet aims to enhance relative velocity while reducing absolute velocity through the rotor [22]. The magnitude of rotation and relative velocity are highest at the tip. By setting $C_{\theta 1}$ equal to U_1 and $C_{\theta 2}$ equal to 0, the energy equation is simplified when the inlet flow angle relative to the blade is zero and the absolute exit velocity is axial.

$$\frac{\dot{W}_T}{\dot{m}} = U_1^2 \tag{3}$$

The blade speed directly influences the specific work output. Designers typically adhere to a maximum value for U_1, which is determined by factors such as the rotor material and the turbine's operating temperature. Follows that:

$$\left(\frac{U_1}{a_{01}}\right)\left(\frac{C_{\theta 1}}{a_{01}}\right) = \left(\frac{S_w}{\gamma - 1}\right) \tag{4}$$

The number of turbine blades is given by the empirical correlation from Whitfield and Baines [11], which is given in Eq. (5):

$$Z_B = \frac{\pi}{30}(110 - \alpha_2)\tan\alpha_2 \tag{5}$$

The enthalpy-entropy, *h-s* diagram in Figure 2 represents thermodynamic processes in a radial turbine rotor. Figure 2 shows how energy is transferred or lost during the turbine's operation. Changes in temperature and entropy of the working fluid are illustrated as it passes through the different stages of the turbine. At the initial stage, the fluid flows into the turbine. Changes occur as the fluid moves through the turbine, as illustrated by state points 1, 2, 3, and 4. These points represent crucial moments in the flow development throughout the turbine volute (1 – 2), stator (2 -3) and rotor (3 – 4). In the ideal case where entropy remains constant, it is called an isentropic process, such as 1 – 3 and 3 – 4 on the h-s diagram, indicating an isentropic fluid expansion through the turbine as a subscript of is. However, in the actual process, losses occur due to friction, turbulence, and other heat losses, increasing entropy, as illustrated by the curved lines from 1 to 3 and 3 to 4 [7], [23]. The *h-s* diagram is useful for determining the rotor design, cooling systems, and working conditions of the radial turbines. Through entropy changes and temperature drops, optimisation and modifications can be made to reduce losses and maximise efficiency.

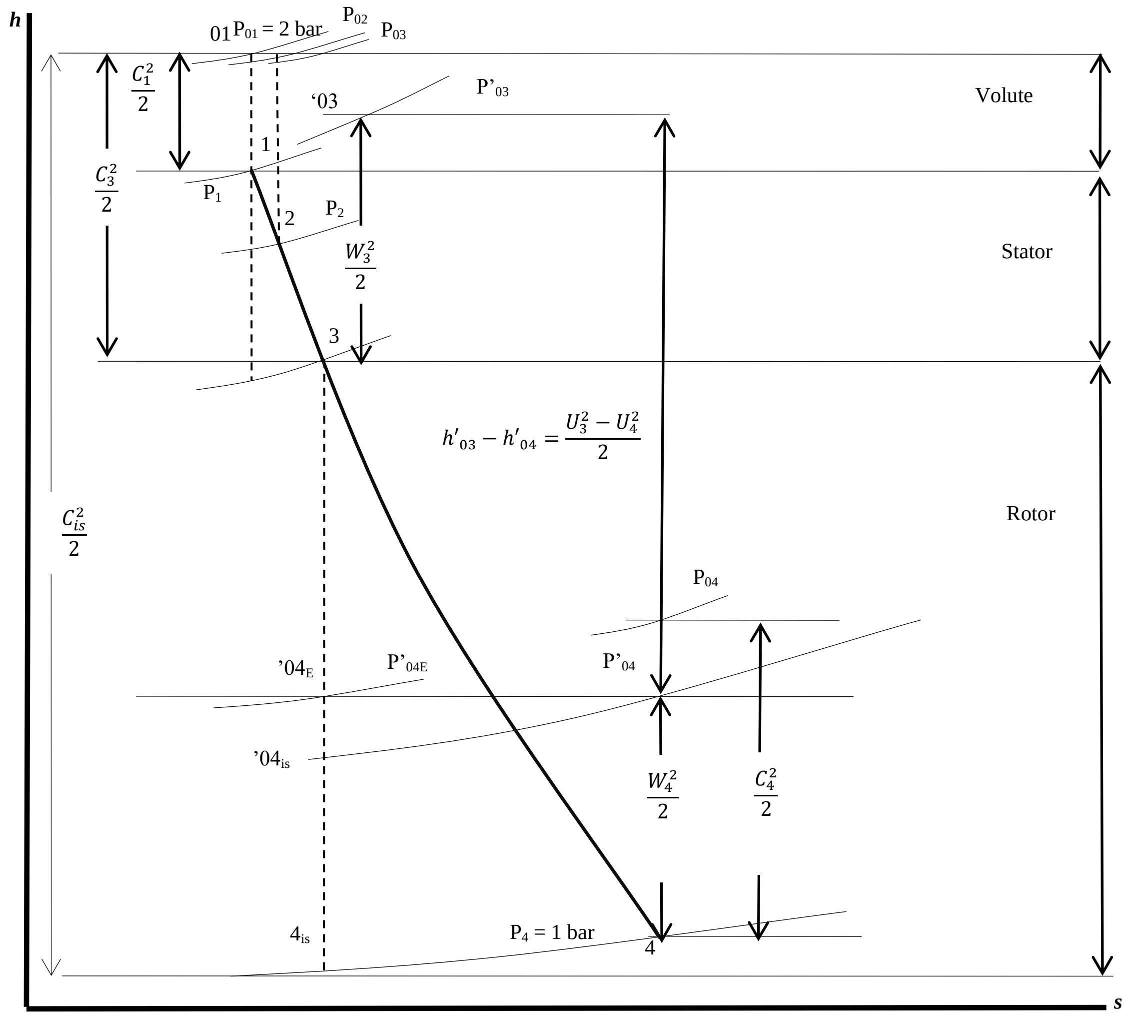

Figure 2. Enthalpy-entropy diagram

2.1.1 Rotor Design Parameters

The rotor design process is fundamental to ensure the turbine's performance and efficiency. The key design parameters that were obtained from the preliminary analysis are discussed in this section. The inlet conditions, including mass flow rate, pressure ratio, total pressure, inlet temperature, and turbine power output, are crucial for conducting a numerical analysis of the radial turbine design. The operating conditions for the radial turbine are given in Table 1, where the variables are used to derive the key parameters of the turbine. The parameters such as the Mass Flow Parameters, *MFP*, Pressure Ratio, *PR*, Specific Speed, *SP* and Total-to-static Efficiency, $\eta_{T\text{-}s}$ must be defined to guide the design process in the initial stage of the design to guide the designer in identifying the turbine's operation and performance [11],[24].

Table 1. Turbine design parameters

Items	Specifications
Mass flow rate, $\dot{m}$ (kg/s)	0.025
Rotation speed, N (rpm)	70 000
Power output (W)	500
Pressure ratio, PR	2
Inlet temperature (K)	800
Inlet Pressure (kPa)	200

2.2 Three-Dimensional Modelling

Three-dimensional (3D) surface modelling of radial turbines is a complex process that involves creating turbine components using computer-aided design (CAD) with precision and detail. In the initial design stage, evaluating the turbine's performance has generated insights into the turbine's physical design, and it is essential to create a virtual 3D prototype. The process of 3D modelling begins with a conceptual design phase, where the general geometry of the turbine and key parameters, such as blade size, rotor, and casing, are defined. The use of CAD software can assist designers in producing accurate 3D models of each component, including complex curvatures and surfaces of turbine blades, using commercially available software such as CATIA, SolidWorks, or Autodesk Inventor. Blade geometry generation, angles, and thicknesses are calculated, and the curvatures are created using Bezier Polynomials. Assisting numerical tools, such as MS Excel, are used to develop complex algorithms, and the blade profiles can be initially visualised.

Bezier polynomials, which aid in producing smooth curvatures for various applications, including computer graphics, animation, industrial design, and turbomachinery blades, are powerful mathematical formulations. A Bezier polynomial is a formula displaying a curvature controlled by a series of control points. The generated curvature does not pass through all the control points, but they influence it, thus making a smooth curve. The number of Bezier degree orders determines the number of control points. A fourth-order Bezier polynomial is defined using five control points: $P_0, P_1, P_2, P_3,$ *and* P_4. In this project, the fourth-order Bezier curvature was selected to produce the meridional and camberline curvatures, which are given by Eq. (5).

$$B(u) = (1-u)^4 p_0 + 4(1-u)^3 u p_1 + 6(1-u)^2 u^2 p_2 + 4(1-u) u^3 p_3 + u^4 p_4 \tag{5}$$

where u ranges between 0 and 1while the binomial coefficients become the control points, that is given as $P_0, P_1, P_2, P_3,$ *and* P_4. Each of the terms in Eq. (5) forms a point on the curve and generates a smooth curvature that does not pass through the given control points. Adjustments of the control point easily modify the curvature. The curvatures of the hub and shroud are easily modified by adjusting the control points. Additionally, the camberline profile can be created using Eq. (5), which can produce complex shapes and surfaces, such as the radial turbine passage and turbine blade profile, that meet the desired aerodynamic requirements.

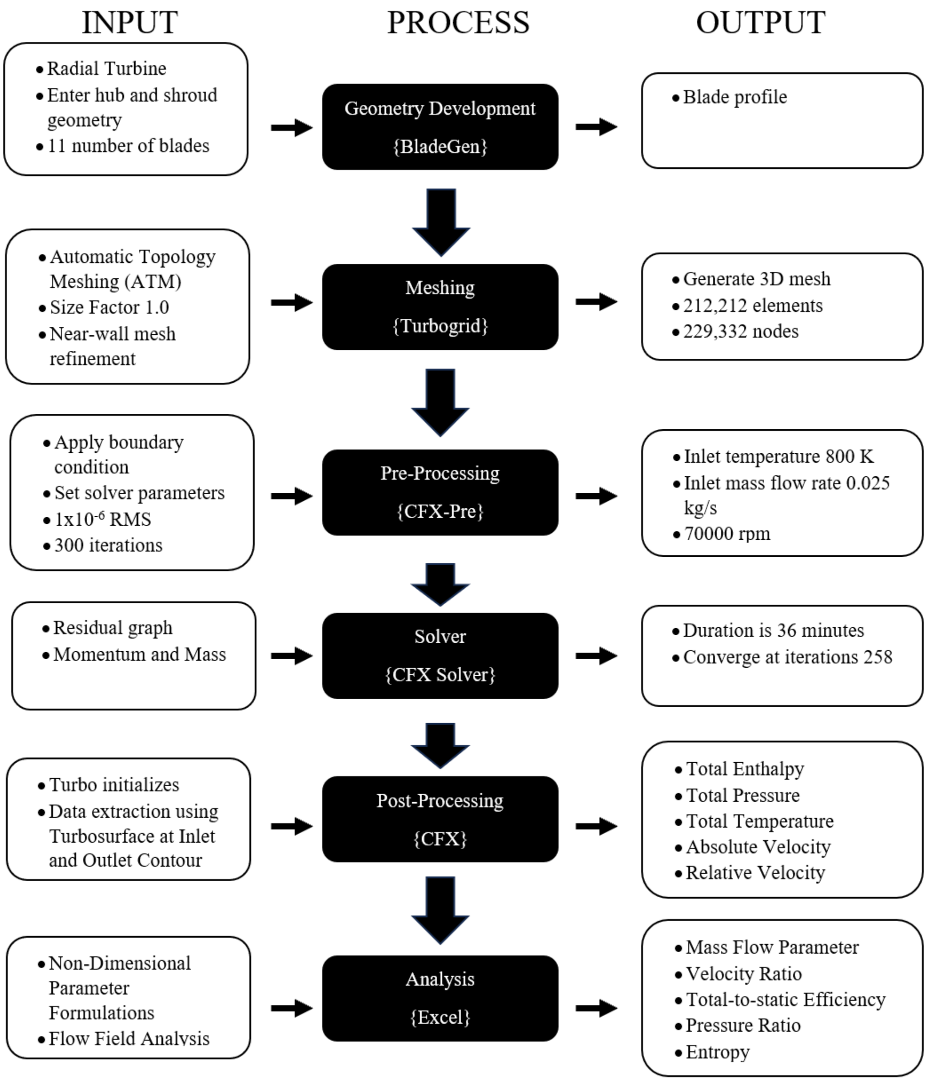

Figure 3. Flowchart of the CFD Procedures in Ansys CFXs

2.3 Computational Turbine Performance Set Up

The purpose of computational analysis is to simulate and analyse the performance and flow field pattern around the high-pressure turbine by using Computational Fluid Dynamics (CFD) software as a tool. There are several processes required to evaluate a high-pressure turbine, including Geometry Generation (Bladgen CFX), Mesh Generation (Turbogrid), Pre-Processing (Pre-CFX), Solver (ANSYS CFX), Post-processing, and Data Extraction, where all the data will be obtained. Figure 3 illustrates the flowchart for the procedures in Ansys CFX for the CFD analysis. The governing equations for fluid flow are derived from the fundamental principles of mass conservation, momentum conservation, and energy conservation, which are known as the RANS equations for the turbulent flow model in the CFD analysis. The Eddy Viscosity Model (EVM) was employed to model the turbulent flow in the radial turbine.

2.3.1 Geometry Generation (BLADEGEN CFX)

The turbine impeller's blade profile will be created in the first stage, utilising ANSYS BladeGen as the modeller and the design requirement measurement. As illustrated in Figure 4(a), the hub and shroud geometry of the blade profile will be input into the meridional form coordinates. At the inlet, the hub radius, r_{1h}, was set up at Z = 0. Moving horizontally along the shroud, the radius remains constant at Z to create a leading edge (LE) section. As the curved section progresses, the shroud radius, r_{1s}, decreases, with significant points at Z, where the radius transitions to create the trailing edge (TE). The blade thickness is fixed to 1 mm. Furthermore, 10 to 11 blades were incorporated into the total rotor design. These variables are essential for delineating the blade's principal geometrical characteristics. As Figure 4(b) demonstrates, a blade-to-blade graphical user interface is used to visualise and fine-tune the blade shape for the camberline, pressure surface, and suction surface curvature.

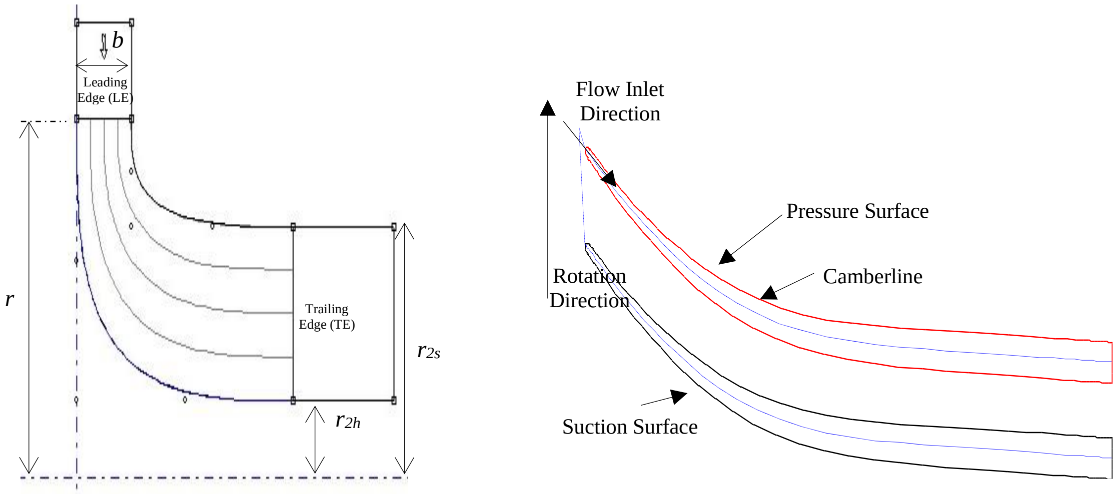

(a) (b)

Figure 4. (a) Meridional view and (b) Blade-to-blade the generated camberline

2.3.2 Mesh Generation

Meshing, the technique of splitting the computational domain into discrete, small pieces called cells, is crucial to Computational Fluid Dynamics (CFD) simulations. The quality of the mesh directly impacts the accuracy and effectiveness of the simulation. A good mesh should have the right element size, aspect ratio, skewness, and orthogonality to produce correct results. It features capabilities such as automated refinement, structured meshing for turbomachinery components, and hybrid meshing for complex geometries. ANSYS TurboGrid was used in the meshing process to create a mesh with 212,212 elements and 229,332 nodes for the high-pressure turbine component. Figure 5 shows the single-passage mesh elements generated using TurboGrid. The meshing parameters are related to the computational fluid dynamics (CFD) aerodynamic modeling of a turbine blade. This single-passage method is similar to Fattah et al. [17].

To create meshing elements for a complex geometry, such as the radial turbomachinery passage, the Advancing Front Method (AFM) in the Topology Mesh Technique—a progressive and adaptive meshing procedure—can be utilized in the TurboGrid setup. The original mesh size should serve as the baseline when the Size Factor value is set to 1. The Boundary Layers Refinement Control function is based on mesh size. It creates a finer mesh near the boundary layers to capture intricate flow features and improve accuracy in crucial areas. Due to its proportionality, the Spanwise Blade Distribution Parameter is generated at a constant resolution by adjusting the mesh distribution along the blade's span according to the blade's geometry. The Hub Tip Mesh Method, which matches expansion at the blade tip, can be used to maintain the mesh quality and accuracy of the simulations. The method ensures that the mesh grows smoothly and consistently from the hub to the tip. The mesh setup parameters are listed in Table 3.

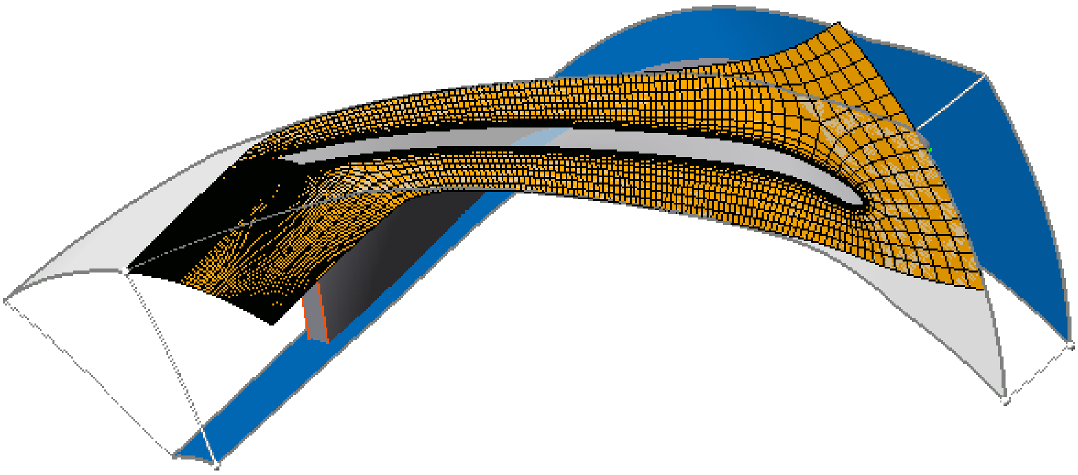

Figure 5. The meshing of a single passage

Table 2. Meshing set-up parameters

Parameter	Method
Topology Mesh Technique	ATM
Size Factor	1
Boundary Layers Refinement Control	Proportional To Mesh Size
Spanwise Blade Distribution Parameter	Proportional
Hub Tip Mesh Method	Match Expansion at Blade Tip
Near Wall Treatment	Absolute

2.3.3 Pre-Processing

The pre-processing in the CFD software involves setting up the model and simulation environment before conducting the analysis. The process involves importing or generating the geometry, assigning material attributes, and dividing the geometry into finite elements to create a mesh. Table 3 depicts the solver setup in the pre-processing for the Ansys CFX. The fluid is described as air and is modelled as an ideal gas during the preprocessing stage of the simulation. The assumption simplifies the behavior of the working fluid by assuming a linear relationship between pressure, volume, and temperature. The baseline pressure for the simulation is the reference pressure, which is set at standard atmospheric pressure or 101,325 Pa. For the simulation to utilize all equations for energy, including kinetic and thermal energy, the Total Energy technique, which represents the heat transfer process, was employed. A widely used turbulence model, the k-e model, was selected for predicting turbulence flow in the CFD simulation [25]. The k-ε turbulence model strikes a balance between accuracy and computational efficiency for various flow conditions. The Model solves two transport equations for the turbulent kinetic energy (k) and its dissipation rate (epsilon). This configuration ensures a thorough and precise representation of heat transfer and fluid dynamics within the system under study. The Ansys CFX uses the Finite Volume Method (FVM) to discretize the k-ε turbulence.

Table 3. Solver set-up

Parameter	Method
Fluid	Air Ideal Gas
Reference Pressure	1013,25 Pa
Heat Transfer	Total Energy
Turbulence Model	k-Epsilon

Important sections of the turbomachinery model for simulation are defined by the "Region Information" settings in Turbo Mode within ANSYS. The inner and outer boundaries where the blades are joined and encased are denoted by the terms "Hub" and "Shroud". The actual blades are specified in the "Blade" area. The "Inlet" and "Outlet" limits show where the fluid enters and leaves the domain. Assuming that the machinery repeats around the circumference, "Periodic 1" and "Periodic 2" define periodic boundaries for modelling a section of the machinery. The absence of matching between "Symmetry," "Tip 1," and "Tip 2" suggests that no particular symmetry planes or tip clearances are used in this configuration. Table 4 shows the boundary conditions set up at the inlet and outlet of the fluid passage for the radial turbine. The thermal condition of the fluid entering the system is defined by the total temperature (T-Total), which is 800 K in the preprocessing configuration for the ANSYS simulation. The mass flow rate is applied to specific geometric passages or sections since the mass flow parameter is specified per passage. With a mass flow rate of 2.3 g/s, the fluid entering each route each second is precisely specified at the passage's inlet and outlet, as shown in Figure 6. By defining the flow direction as normal to the boundary (refer to Figure 6), which means that the fluid enters perpendicular to the designated boundary surfaces, the boundary condition is made simpler, and the simulation's accuracy is increased by guaranteeing a consistent entry flow. To effectively describe the fluid dynamics and thermal characteristics within the system, the thermal and flow parameters must be specified in detail.

Table 4. Boundary conditions set-up

Parameter	Method
T-Total	800 K
Mass Flow	Per Passage
Mass Flow Rate	0.5 2.3 $g.s^{-1}$to 10 $g.s^{-1}$
Flow Direction	Normal To Boundary
Mass Flow Parameter, MFP	0.0005 – 0.012
Pressure Ratio, PR	1.1 – 1.6
Velocity Ratio, U_2/C_{is}	0.05 – 0.65
Rotational Speed, RPM	50 000; 70 000 & 90 000

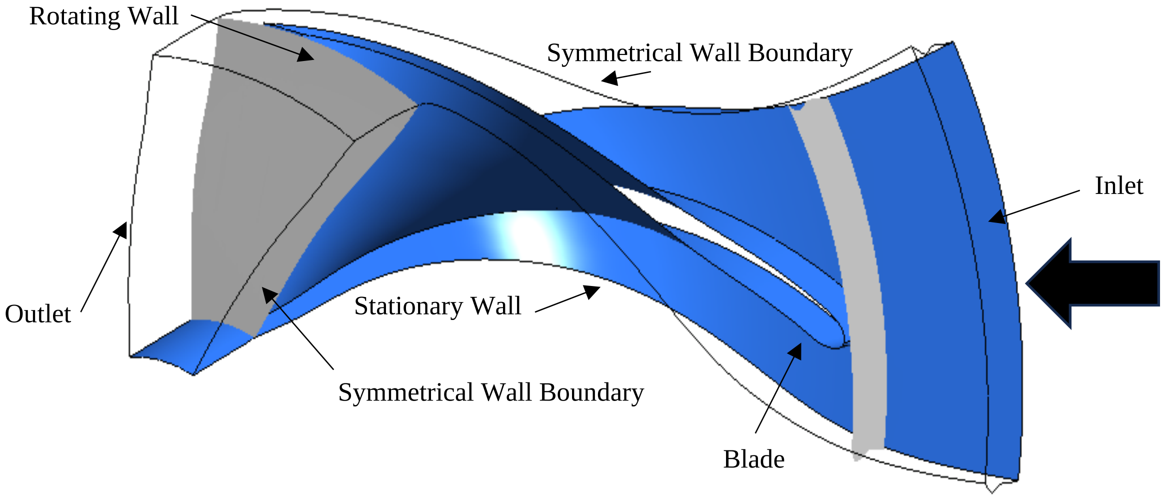

Figure 6. Boundary conditions set-up

3. RESULTS AND DISCUSSION

3.1 Rotor Geometrical Design

Figure 7 represents the relationship between the inlet length and absolute angle. As the α_1 increases from 70° to 80°, inlet length *b* increases from 0.005 m to 0.009 m. A larger inlet angle requires a longer length, likely due to aerodynamic or structural design requirements to maintain efficient fluid flow into the turbine. Comprehending the aerodynamic and structural relationship is important for optimising turbine design. Balancing the desired inlet angle with the physical constraints between the two constraints helps to design the inlet and enhance the overall performance and efficiency of the turbine. The design specification of α_1 at 72° with an inlet length *b* of 0.005 m was selected due to the potential for an optimal balance between the inlet angle and the length required for effective flow. As the inlet absolute angle increases, it changes the alignment of the flow entering the turbine, affecting flow separation and modifying the aerodynamic efficiency. The flow alignment that enters the turbine at the leading edge ensures that the inlet length is sufficient to accommodate the inlet air mass. This leads to smoother flow transition and minimised losses at the inlet. This is consistent with the study done by H. Chen and Baines optimise the flow inlet angles to reduce separation and enhance turbine efficiency [5]. Additionally, increasing the inlet length with an angle helps manage flow distribution and minimizes secondary flow losses, thereby improving performance [26].

Figure 8 illustrates the correlation between the inlet absolute Mach number, M_1, and inlet absolute angle, α_1, for the specified radial turbine design. Figure 8 shows that the M_1 decreases as α_1 increases. As the angles of the inlet further increase, the bulk airflow that enters the radial turbine, known as meridional velocity, C_{m1}, is lower, resulting in lower Mach numbers. The value of α_1 is 72°, with M_1 is 0.267, which is selected as a design parameter. A higher Mach number can lead to shock waves and higher losses, while a lower Mach number may not generate sufficient energy for the turbine. Varying the inlet angle influences the Mach number, pressure, and velocity profiles entering the rotor. Lower Mach numbers at higher angles help reduce shock losses, enhancing turbine efficiency.

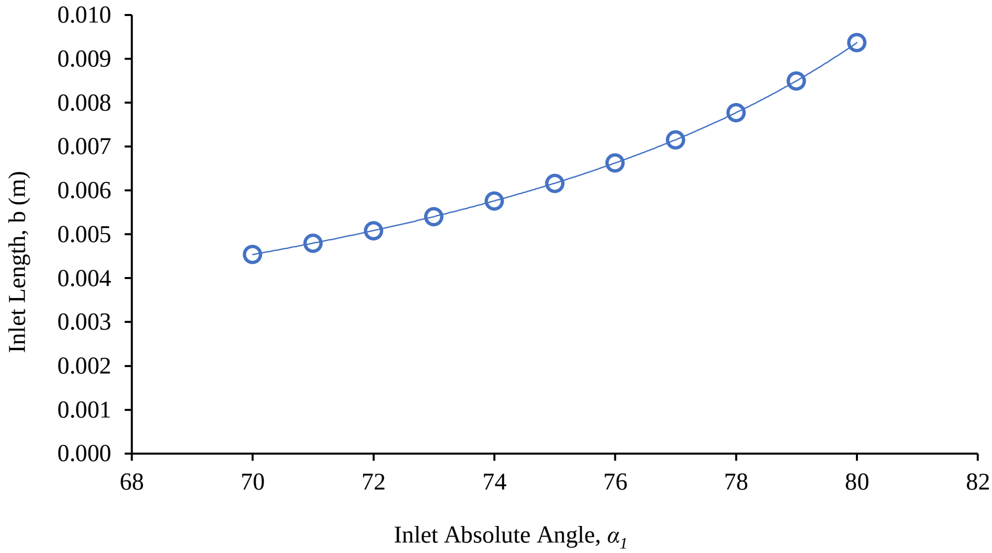

Figure 7. Inlet length at various inlet absolute angles

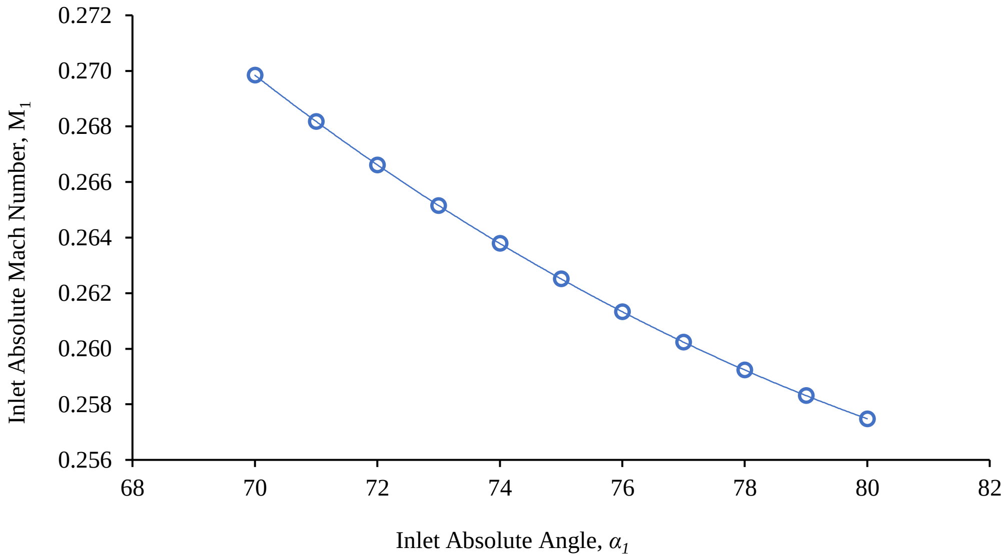

Figure 8. Inlet absolute Mach number at various inlet absolute angles

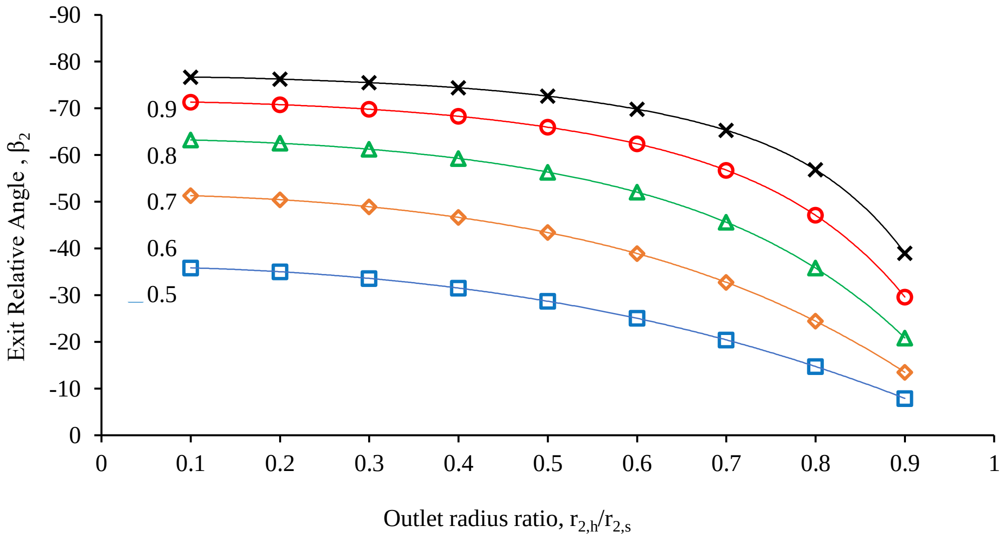

Figure 9. Exit relative angle at various $r_{2,h}/r_{2,s}$

The effect of the exit relative angle, β_2, is shown in Figure 9, which illustrates a significant decrease in β_2 as the outlet radius ratio, $r_{2,h}/r_{2,s}$, increases. A higher value of β_2 and $r_{2,h}/r_{2,s}$ will increase the relative velocity and decrease the rotor's height at the exit, respectively. Also, Figure 9 depicts the effect of the ratio of the exit radius shroud to the inlet radius, $r_{2,s}/r_1$. The value of $r_{2,s}/r_1$ must be less than 1.0. Figure 9 also shows that β_2 increases as $r_{2,s}/r_1$ increase. The highlighted value β_2 of -61°, when $r_{2,h}/r_{2,s}$ = 0.7, represents the chosen design parameter, optimizing the relative angle for efficient exit flow conditions. This design aims for favourable exit flow conditions with minimised flow separation and aerodynamic losses. In the design point selection, it is essential to optimize the exit angle to control swirl velocity and enhance the alignment of the exit flow with downstream components. Reducing the exit angle achieves a smoother flow transition, reducing losses and improving efficiency [27].

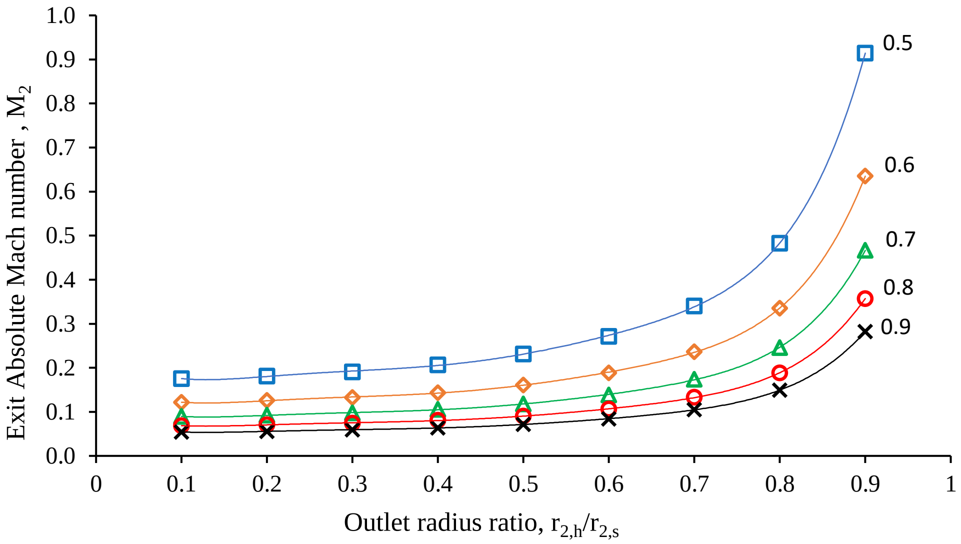

Figure 10. Exit Absolute Mach number, M_2 at various $r_{2,h}/r_{2,s}$

Figure 10 shows that the exit absolute Mach number, M_2, is increased as the $r_{2,h}/r_{2,s}$, is increased and the $r_{2,s}/r_1$ is decreased. At $r_{2,h}/r_{2,s}$ equals 0.7 and $r_{2,s}/r_1$ equals 0.7, and the value M_2 is 0.1. It can be observed that the absolute velocity decreases at the exit of the turbine rotor. A lower M_2 will contribute to a larger operation ratio for the turbine rotor. Optimising the exit Mach number is important to ensure efficient turbine operation without excessive shock losses or flow distortions. Higher exit Mach numbers improve the turbine's expansion process but must be managed to avoid adverse performance effects [28].

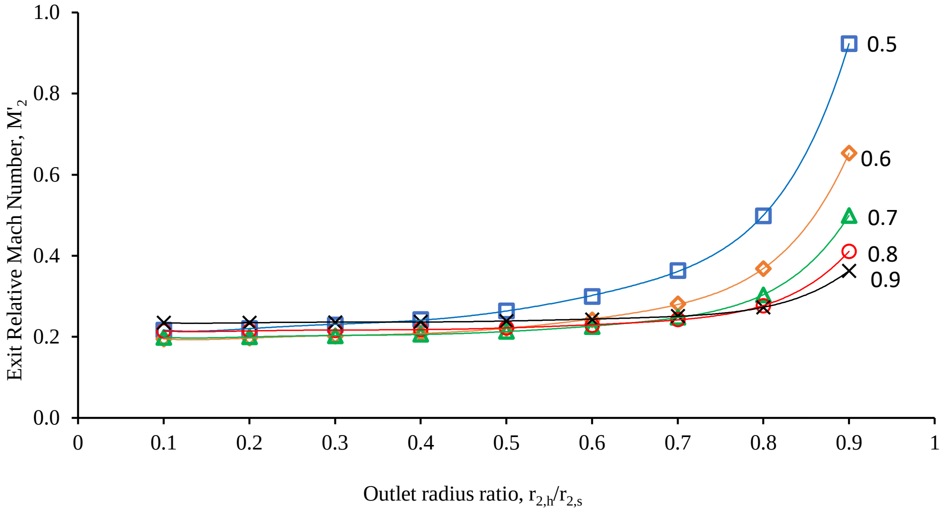

Figure 11. Exit relative Mach number, M'_2 at various $r_{2,h}/r_{2,s}$

Figure 11 shows that the exit relative Mach number, M'_2, varies with design parameters of $r_{2,h}/r_{2,s}$, showing an increasing proportion to the exit relative Mach number. Also, the M'_2 is increased as the $r_{2,s}/r_1$ is increased. The value of M'_2 is 0.2 for $r_{2,h}/r_{2,s}$ of 0.7 represents the chosen design parameter. The selected value influences the relative flow speed at the turbine exit. Despite a large relative, β_2, the relative velocity is low at the rotor exit. This exit condition suggests an optimised design sizing of the rotor to manage relative velocities and reduce aerodynamic loading on rotor blades. Managing the relative Mach number minimises velocity losses and improves energy conversion efficiency. Maintaining balanced relative Mach numbers ensures optimal aerodynamic and structural performance limits for the turbine [29]. Finally, the physical characteristics of the turbine can be identified from the analysis conducted in Figures 7 to 11. Table 2 shows the design specifications. The flow at the exit of the turbine was set to be axial; thus, the $\alpha_2 = 0$. The number of blades was determined using Eq. (5), and the turbine has 11 blades. The thickness of the blade is 1.0 mm, and the blockage factor, *B*, is 20%.

Table 2. Results of turbine design parameters

Items	Specifications
Inlet radius, r_1 (mm)	19.3
Length of leading edge (mm)	4.5
Inlet absolute angle, α_1 (°)	72
Exit radius ratio, $r_{2,h}/r_{2,S}$	0.7
Exit relative angle, β_2 (°)	-61
Number of blades	11
Thickness of blades (mm)	1
Blockage factor, *B* (%)	20

Figure 12(a) shows the camberline of a rotor for a radial turbine. Camberline is one of the important parameters of blade design, which means the line along the blade from the leading edge to the trailing edge. The camber line graph shows the curvature profile of the blade along its length. The curve originates from the origin, representing the blade's leading edge, with a constantly increasing slope that indicates the degree of curvature of the blade. The steep slope indicates a high camber towards the rear edge, ensuring proper airflow through the turbine. This camber line design is critical for improving the aerodynamics of the turbine blade, minimising flow separation, and raising efficiency [10]. Figure 12(b) shows a meridional section of a rotor. The curvatures were generated using the Bezier polynomial equations, which are widely used in aerodynamic design and produce smooth curves. This was employed to define the geometry of the rotor blade in different sections. The outermost curve refers to the hub section of the rotor and goes to the shroud. A meridional section graph using Bezier curves helps outline the blade, maintaining a smooth flow.

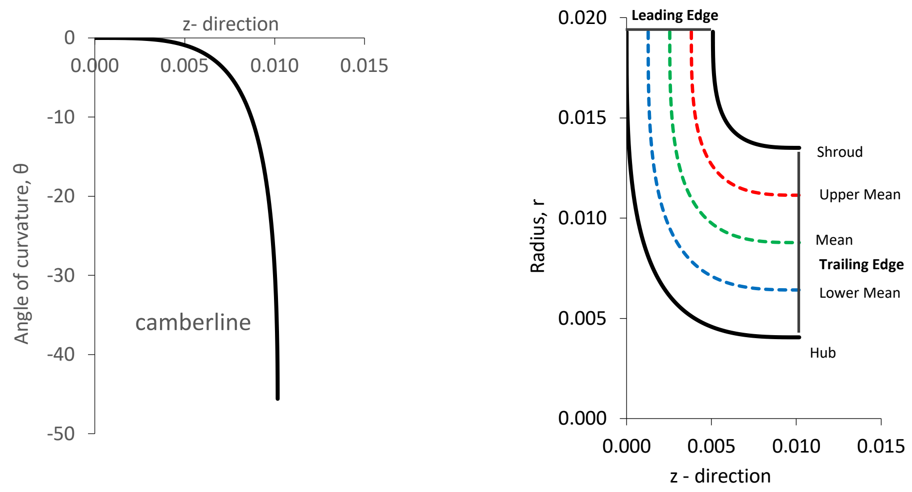

Figure 12. Curvature for the turbine rotor: (a) Camberline and (b) Meridional

3D geometry involves representing objects or shapes within a three-dimensional area. In contrast to 2D geometry, which focuses on flat shapes, 3D geometry includes depth, width, and height to create a more realistic depiction of objects. The use of CATIA for geometric design is often compared to other software tools. For example, integrating CATIA with MS Excel and Autodesk Inventor can enhance the overall design workflow, providing a comprehensive solution for creating detailed and complex geometries. This synergy is particularly advantageous for optimising design parameters and improving the manufacturability of turbine components [30]. The basic geometric layout of the radial turbine rotor was defined. The outline was developed using initial calculations and design principles. The blade profile stood out as an important element of the rotor configuration. Following the initial establishment of the outline structure, a detailed design was done to enhance the geometry. This involved utilizing CATIA's surface modeling tools, generating seamless surfaces for the blades of each part. The distribution of the turbine blades is shown in Figure 13, illustrating their positioning around the rotor hub. This condition was commonly observed in radial turbines, where the blades were positioned relative to each other from a central point, allowing the fluid to pass through in a radial flow pattern within the turbine. The arrangement ensured that the flow was distributed evenly, thereby increasing the turbine's performance. The 3D geometric configuration of a radial turbine rotor was developed and constructed. This emphasised capturing the detail of blade profiles. The turbine's rotor was drawn in every detail to ensure the viewer understood how the device worked and its main components. During the modelling process, three-dimensional computer-aided design software was used to create the turbine. The final model of the radial turbine rotor is a 3D model. Moreover, it emphasised the significance of the accurate geometric design of blades in radial turbines and paved the way for further innovations and developments.

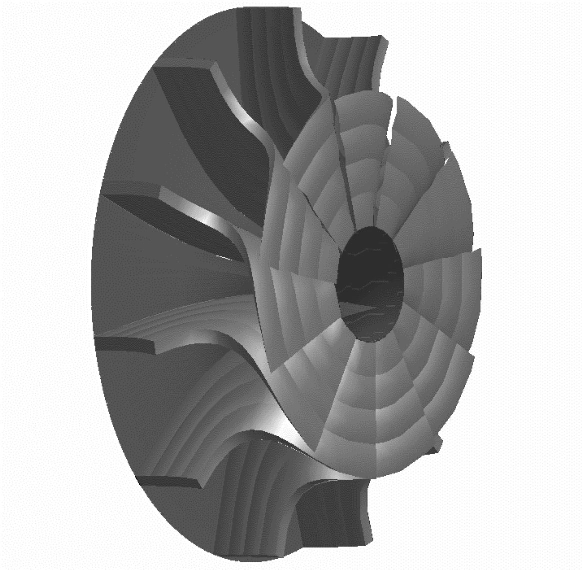

Figure 13. 3D model of the turbine rotor

3.2 Computational Performance

The performance map in Figure 14 illustrates how the Mass Flow Parameter (MFP) of a radial turbine varies with Pressure Ratio (PR) at different rotational speeds (50,000 RPM, 70,000 RPM, and 90,000 RPM). The map trend is a common trend Whitfield published [11]. As PR increases, MFP rises for all speeds, but the increase is more pronounced at lower PRs. At 50,000 RPM, the turbine can handle the highest mass flow, making it the most efficient speed. However, as the RPM increases to 70,000 and 90,000, the radial turbine's ability to handle mass flow decreases, likely due to increased aerodynamic and mechanical losses. The performance map also hints at the phenomenon of choking. Choking occurs when the turbine reaches a point where increasing the PR further does not result in a higher mass flow, as the flow speed reaches the speed of sound; consequently, the exit relative velocity discharge is greater than the inlet. Figure 14 illustrates this by flattening the curves at higher PRs, particularly at higher RPMs, such as 90,000 RPM. The designed turbine is choked approximately at PR≈1.4, as observed. At this point, the turbine cannot pass more mass flow, regardless of further increases in PR, signalling the onset of choking. The flow limitation has reduced the turbine's performance, as its efficiency drops and it can no longer increase its output.

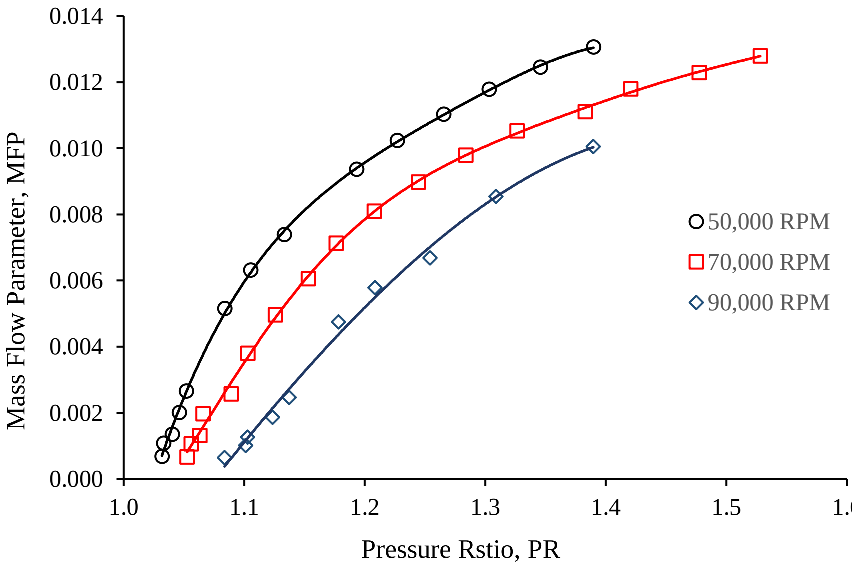

Figure 14. Pressure ratio versus mass flow parameter

Figure 15 shows the Total-to-Static Efficiency, η_{T-s} , of a radial turbine as a function of the Velocity Ratio, U_2/C_{is}, for three different rotational speeds: 50,000 RPM, 70,000 RPM, and 90,000 RPM. The efficiency increases with the velocity ratio, reaches a peak, and then declines, forming a parabolic curve for each speed. The highest efficiency is achieved at 70,000 RPM, peaking at around 67% at a velocity ratio of approximately 0.4. For 50,000 RPM, the peak efficiency is slightly lower, around 55%, while at 90,000 RPM, the maximum efficiency is about 60% at a higher velocity ratio. These observations highlight the optimal operating point for each speed, where the turbine performs most efficiently in converting kinetic energy into useful work. The efficiency trends observed in the graph are significantly influenced by aerothermodynamic effects, which encompass the interactions between thermal and aerodynamic processes within the turbine [28]. As the bulk air increases, the relative velocity of the working fluid also increases, leading to changes in the turbine's temperature, pressure, and velocity fields. These changes impact the thermodynamic cycle and aerodynamic losses, ultimately affecting the overall efficiency.

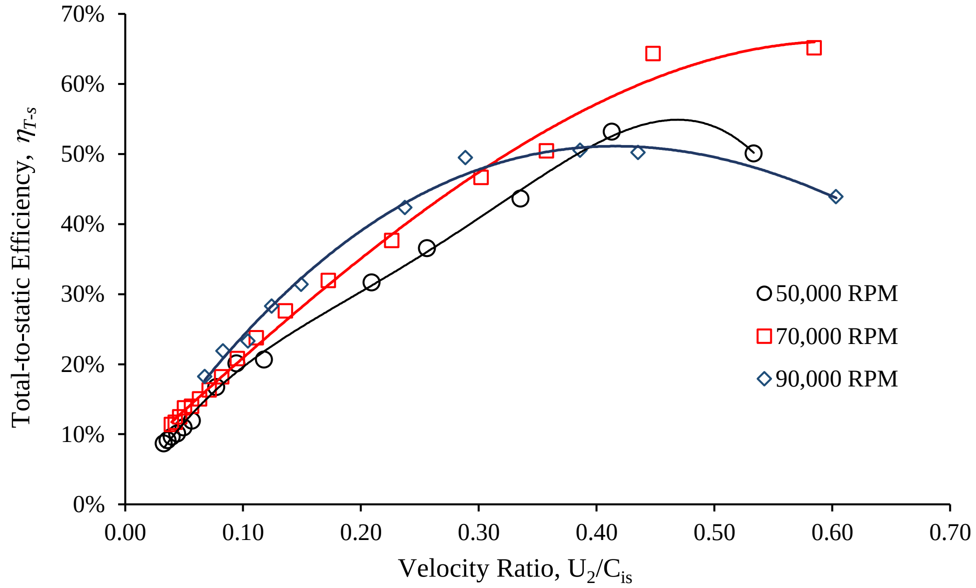

Figure 15. Total-to-static efficiency at various turbine speeds

At higher rotational speeds, such as 90,000 RPM, the increased velocity of the working fluid raises the total temperature, leading to higher heat losses through conduction, convection, and radiation. The rise in temperature affects air properties, such as density and viscosity, according to CFD modelling, which treats air as an ideal gas. The temperature rise has increased friction and flow separation, including secondary flow and velocity gradients. Subsequently, it increases aerodynamic loss. The effect of flow separation becomes more significant at higher speeds due to the increased centrifugal force, which can contribute to shock losses in the relative flow and further reduce efficiency after the peak velocity ratio is reached. These losses are reflected in the sharper decline in efficiency observed at 90,000 RPM compared to lower speeds.

The turbine performance depends highly on the α and *i* at the turbine inlet [5]. Japikse suggested that the optimum range for *i* at the leading edge of the turbine is $-20 \leq i \leq -40$ [31]. The *α* is the angle at which the flow enters the turbine blades relative to the axial direction, while *i* is the angle between the incoming flow and the blade's leading edge (refer to Figure 1). Both angles significantly impact the efficiency by influencing the aerodynamic loading on the blades and the flow behaviour within the turbine [5, 29, 31]. At lower velocity ratios, where PR is relatively high, the incidence angle tends to be out of the optimum range, leading to unfavourable flow conditions with higher flow separation and greater aerodynamic losses. This condition is generally associated with lower efficiencies. However, the pressure ratio decreases as the velocity ratio increases, and the bulk velocity reduces at the leading edge. This condition can move the *i* into the optimum range and increase the η_{T-s} until a maximum value is reached. As the mass flow decreases and *PR* decreases, the *α* and *i* increase significantly. Subsequently, the η_{T-s} has dropped significantly.

The identification of design *α* is also to complete the radial turbine's design. The *α* is determined by the volute cross-sectional area in the radial turbine [8]. If the *α* is not optimised for a given design speed, the flow can enter the turbine blades at too steep or shallow an angle, leading to non-optimal flow conditions at the leading edge. A higher *α* can result from increased aerodynamic loading on the blades, leading to higher frictional losses and potential blade vibration or fatigue. In contrast, a smaller *α* results in insufficient aerodynamic loading, reducing the extraction of exhaust energy. In Figure 16, the differences in peak efficiency at various rotational speeds can be partially attributed to variations in the *α* and *i* angles at the turbine inlet. At 70,000 RPM, the turbine operates with an optimal combination of *α* and *i* angles, leading to the highest efficiency. At 50,000 RPM and 90,000 RPM, where the prior has a higher mass and the latter has a lower mass, the deviation from these optimal angles could result in higher aerodynamic losses and lower peak efficiencies.

3.3 Flow Field Analysis

A detailed investigation of physical properties, such as pressure, static entropy, and velocity, within the flow passages is necessary to understand the turbine aerodynamic flow field in CFD analysis. Velocity refers to the magnitude and direction of fluid flow, which is crucial for understanding the behavior of fluid flow on rotor surfaces. Analyzing the wake zones where velocity decreases due to flow separation or energy extraction is important to improve the blade design. The interaction of air molecules in the rotor passage creates variations in fluid velocities. As the fluid approaches the rotor surface, the effect of the boundary layers becomes more significant because the friction increases near the surface. Understanding the fluid behaviour will enhance turbine design, as it can further optimise energy extraction and identify solutions to increase the operating performance of the turbine.

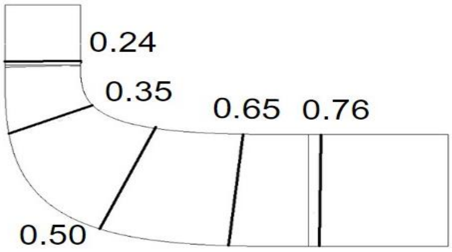

Figure 16. Spanwise cross-section location

The disorder of fluid molecules in fluid dynamics is referred to as static entropy, another important parameter in measuring the energy conversion efficiency of a turbine. An effective energy conversion is indicated by a lower entropy change across the rotor blades; conversely, a higher entropy region outlines the energy losses due to several possible flow phenomena, such as shock waves, turbulence, or friction. The effect of the entropy generated is depicted in Figure 2, where the entropy generated has decreased the energy output from the gas expansion process in the turbine. The static entropy contour can be visualised in the turbine passage. Figure 16 shows a cross-sectional view of a turbine blade, with specific measurements at various segments (0.76, 0.65, 0.50, 0.35, 0.24) along its spanwise direction. These measurements, extending from the root to the tip, are essential for evaluating the turbine's structural integrity, power output, and efficiency. By summing the segment measurements, one can determine the overall span size of the blade, which plays a crucial role in the blade's aerodynamic performance.

Figure 17 shows the flow field analysis at various cross-sections in the spanwise direction of the turbine. The study was conducted at the design point, where the mass flow rate is 0.025 kg/s and the rotational speed is 70,000 rpm. The performance analysis of a high-pressure turbine offers crucial insights into the thermodynamic and mechanical processes that govern the expansion process within the turbine. One of the key indicators of performance is the change in the working fluid's total enthalpy, which decreases from 504,757 J/kg at the turbine's intake to 511,681 J/kg at the outflow. This reduction in enthalpy reflects the turbine's ability to extract energy from the fluid, most of which is converted into mechanical shaft work that drives electrical generators or subsequent turbine stages.

The velocity in the rotor passage changes significantly, increasing from 61.5 m/s at the inlet to 129.7 m/s at the turbine outlet. The acceleration of the working fluid has decreased the pressure from the inlet to the outlet. Subsequently, the flow converts the pressure energy into kinetic energy. The expansion process demonstrates the turbine's efficiency in producing mechanical energy. The intercorrelation between fluid dynamics and thermodynamics is shown by the variation in velocity and its effect on static entropy at different turbine blade sections. The effect of the flow vorticity on static entropy reveals that the velocity gradient patterns have significantly influenced the energy conversion efficiency [18]. At the root section (0.24), the average velocity is relatively low because of the inlet condition where the total pressure is higher. Additionally, the static entropy at this span is low, indicating effective energy transmission with reduced turbulence and aerodynamic loss—the effect of the $\eta_{T-s}$is quantified by the amount of entropy generated in the fluid flow passage. The higher the entropy generated, the lower will be theη_{T-s}. Therefore, the blade profile of the radial turbine must be optimized to reduce the aerodynamic interaction that controls the velocity gradient in the flow passage. A higher velocity gradient contributes to higher entropy generated in the flow passage.

The passage velocity increases as the flow progresses toward the mid-span (0.35 to 0.50 span), generating higher aerodynamic forces and more complicated flow patterns. A more complex flow pattern increases static entropy, indicating greater energy loss due to turbulence. By the mid-span, a significant aerodynamic loading due to increased fluid acceleration has increased the entropy. The continued drop in total pressure and the rise in static entropy, resulting from increased flow turbulence, have made this mid-span region a prominent zone of energy dissipation. Approaching the tip from a span of 0.65 to 0.76, the fluid velocity reaches its maximum value, leading to the most significant aerodynamic interactions and the highest levels of static entropy, especially near the blade tip, which corresponds to the highest turbulence and the weakest area of energy conversion. The blade also experiences the highest aerodynamic forces at this region, resulting in significant energy dissipation and the lowest total pressure.

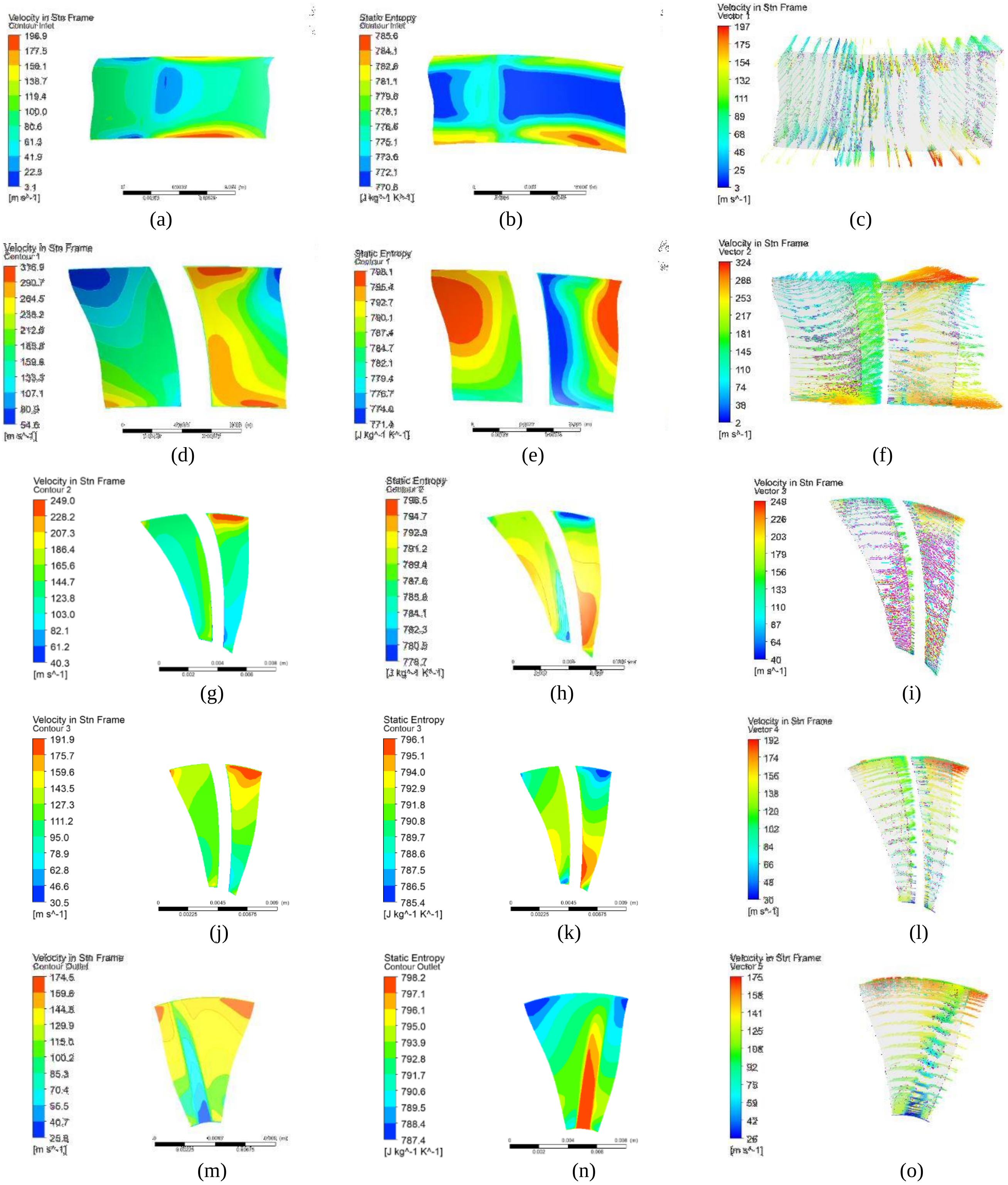

Figure 17. The absolute velocity, static Entropy, and velocity vector analysis in various cross sections: (a-c) 0.24 span, (d-f) 0.35 span, (g-i) 0.5 span, (j-l) 0.65 span, and (m-o) 0.76 span

4. CONCLUSION

This paper presents a comprehensive design methodology, incorporating numerical analysis and optimization, of a 500W high-pressure radial turbine. The main energy source is from the exhaust gas of a single-cylinder internal combustion engine. The fundamental thermodynamic principles and Euler turbomachinery equations were employed to optimise the physical dimensions of the radial turbine. The CFD simulations conducted at varying rotational speeds (50,000, 70,000, and 90,000 RPM) evaluated critical insights into the turbine's performance, with a peak total-to-static efficiency of 67% observed at 70,000 RPM. The paper’s findings emphasise the significance of precise geometric and aerodynamic optimisation in achieving high efficiency in radial turbines. The flow field analysis further highlighted the importance of managing velocity gradients and static entropy within the rotor passage to minimise energy losses and maximise performance. This research makes valuable contributions to the development of high-performance radial turbines, particularly in applications where efficient energy recovery is crucial.

ACKNOWLEDGMENTS

This study was not supported by any grants from funding bodies in the public, private, or not-for-profit sectors.

CONFLICT OF INTEREST

The authors declare that they have no conflicts of interest.

AUTHORS CONTRIBUTION

N. S. Ahmad (Methodology; Data curation; Formal analysis; Visualisation; Writing - original draft)

M. N. Azman (Methodology; Data curation; Software; Formal analysis; Writing - original draft)

A. M. I. Bin Mamat (Conceptualisation, Validation; Formal analysis; Writing - review & editing; Supervision)

AVAILABILITY OF DATA AND MATERIALS

The data supporting this study's findings are available on request from the corresponding author.

ETHICS STATEMENT

Not applicable

REFERENCES

[1] A. F. Yusop, R. Mamat, M. H. Mat Yasin, O. M. Ali, "Effects of particulate matter emissions of diesel engine using diesel-methanol blends," *Journal of Mechanical Engineering and Sciences*, vol. 6, no. 2, pp. 959–967, 2014.

[2] N. R. Abdullah, N. S. Shahruddin, R. Mamat, A. M. I. Mamat, A. Zulkifli, "Effects of air intake pressure on the engine performance, fuel economy and exhaust emissions of a small gasoline engine," *Journal of Mechanical Engineering and Sciences*, vol. 6, no. 2, pp. 959–968, 2014.

[3] N. Watson, M. S. Janota. Turbocharging the Internal Combustion Engine. 1st Ed. London: The McMillan Press Ltd, 1982.

[4] M. Ingale, H. Kawale, A. Thakre, N. Shrikhande, "Performance enhancement of engine using turbocharger-A review," *International Journal of Creative Research Thoughts*, vol. 6, no. 1, pp. 6–10, 2018.

[5] H. Chen, N. C. Baines, "Analytical optimization design of radial and mixed flow turbines," *Proceedings of the Institution of Mechanical Engineers, Part A: Journal of Power and Energy*, vol. 206, no. 3, pp. 177–187, 1992.

[6] A. M. I. B. Mamat, R. F. Martinez-Botas, "Mean line flow model of the steady and pulsating flow of a mixed-flow turbine turbocharger," in *Proceedings of the ASME Turbo Expo*, vol. 7, no. 246, pp. 2393–2404, 2010.

[7] R. S. R. Gorla, A. A. Khan. Chapter 7: Axial Flow and Radial Flow Gas Turbines in Turbomachinery Design and Theory. 1st Ed. Boca Raton: CRC Press, 2021.

[8] C. Li, H. Chen, Y. Wang, Y. Wei, G. Wu, "An investigation of the effects of volute A/R distribution on radial turbine performance," *Proceedings of the Institution of Mechanical Engineers, Part D: Journal of Automobile Engineering*, vol. 238, pp. 3242–3252, 2023.

[9] C. Li, Y. Wang, X. Li, H. Chen, Y. Wei, G. Wu, "A two-dimensional method for radial turbine volute design," *Proceedings of the Institution of Mechanical Engineers, Part A: Journal of Power and Energy*, vol. 237, no. 1, pp. 33–47, 2023.

[10] L. Jun, X. Jinli, J. Rui, W. Hanbin, "Design and analysis of radial turbine rotor based on Bezier curve method," *International Journal of Research in Mechanical Engineering*, vol. 3, no. 5, pp. 49–54, 2015.

[11] A. Whitfield, "The preliminary design of radial inflow turbines," *Journal of Turbomachinery*, vol. 112, no. 1, pp. 50–57, 1990.

[12] A. M. I. Bin Mamat, R. F. Martinez-Botas, S. Rajoo, L. Hao, A. Romagnoli, "Design methodology of a low-pressure turbine for waste heat recovery via electric turbocompounding," *Applied Thermal Engineering*, vol. 107, no. 4, pp. 1166–1182, Aug. 2016.

[13] A. K. Noughabi, S. Sammak, "Detailed design and aerodynamic performance analysis of a radial-inflow turbine," *Applied Sciences (Switzerland)*, vol. 10, no. 11, pp. 1–15, 2018.

[14] A. A. Ahmad Zahidin, A. M. I. Mamat, A. Romagnoli, "Computational performance of a-100 kW low pressure turbine to recover gas turbine exhaust energy," *Journal of Mechanical Engineering and Sciences*, vol. 13, no. 2, pp. 4777–4793, 2019.

[15] Z. Zulkifli, N. H. Abdul Halim, Z. H. Solihin, J. Saedon, A. A. Ahmad, A. H. Abdullah, et al., "The analysis of grid independence study in continuous dispersion of MQL delivery system," *Journal of Mechanical Engineering and Sciences*, vol. 17, no. 3, pp. 9586–9596, 2023.

[16] E. Septyaningrum, R. Hantoro, I. K. A. P. Utama, J. Prananda, G. Nugroho, A. W. Mahmashani, et al., "Performance analysis of multi-row vertical axis hydrokinetic turbine-straight blade cascaded (VAHT-SBC) turbines array," *Journal of Mechanical Engineering and Sciences*, vol. 13, no. 3, pp. 5665–5688, 2019.

[17] B. Ahmad, A. Fattah, A. M. I. Bin Mamat, "Single passage CFD analysis for non-radial fibre element of low pressure turbine," *Jurnal Teknologi*, vol. 76, no. 5, pp. 67–72, 2015.

[18] A. Borovkov, I. Voinov, Y. Galerkin, R. Kamin, A. Drozdov, O. Solovyeva, et al., "Design, plant test and CFD calculation of a turbocharger for a low-speed engine," *Applied Sciences (Switzerland)*, vol. 10, no. 23, pp. 8344–8352, 2020.

[19] X. Yu, M. Li, G. An, B. Liu, "A coupled effect model of two-position local geometric deviations on subsonic blade aerodynamic performance," *Applied Sciences (Switzerland)*, vol. 10, no. 24, pp. 8976–8985, 2020.

[20] K. I. Hamada, M. M. Rahman, D. Ramasamy, M. M. Noor, K. Kadirgama, "Numerical investigation of in-cylinder flow characteristics of hydrogen-fuelled internal combustion engine," *Journal of Mechanical Engineering and Sciences*, vol. 10, no. 1, pp. 1792–1802, 2016.

[21] M. P. Helios, W. Asvapoositkul, "Numerical studies for the effect of geometrical parameters on water jet pump performance via entropy generation analysis," *Journal of Mechanical Engineering and Sciences*, vol. 15, no. 3, pp. 8319–8331, 2023.

[22] N. N. Bayomi, "Radial turbine design process," *Journal of Science and Technology*, vol. 11, no. 19, pp. 9–22, 2015.

[23] A. F. El-Sayed. Aircraft Propulsion and Gas Turbine Engines. 1st Ed. Boca Raton: CRC Press, 2017.

[24] E. Sauret, "Open design of high-pressure ratio radial-inflow turbine for academic validation," *ASME International Mechanical Engineering Congress and Exposition, Proceedings (IMECE)*, vol. 7, no. 1, pp. 3183–3197, 2012.

[25] B. E. Launder, D. B. Spalding, "The numerical computation of turbulent flows," *Computer Methods in Applied Mechanics and Engineering*, vol. 3, no. 2, pp. 269–289, 1974.

[26] M. Tancrez, J. Galindo, C. Guardiola, P. Fajardo, O. Varnier, "Turbine adapted maps for turbocharger engine matching," *Experimental Thermal and Fluid Science*, vol. 35, no. 1, pp. 146–153, 2011.

[27] A. Mobarak, M. G. Khalafallah, A. M. Osman, H. A. Heikal, "Experimental investigation of secondary flow and mixing downstream of straight turbine cascades," Journal of Turbomachinery, vol. 110, no. 4, pp. 497–503, 1988.

[28] A. Meroni, M. Robertson, R. Martinez-Botas, F. Haglind, "A methodology for the preliminary design and performance prediction of high-pressure ratio radial-inflow turbines," *Energy*, vol. 164, pp. 1062–1078, 2018.

[29] A. Leto, "Radial turbine preliminary design and performance prediction," in *AIP Conference Proceedings*, vol. 2191, no. 1, pp. 1–9, 2019.

[30] G. N. Koini, S. S. Sarakinos, I. K. Nikolos, "A software tool for parametric design of turbomachinery blades," *Advances in Engineering Software*, vol. 40, no. 1, pp. 41–51, 2009.

[31] D. Japikse, N. C. Baines. Introduction to Turbomachinery. 1st Ed. United States: Concepts ETI, 1994.